Polyelectrolyte Complex Membranes Based on Two Anionic Polysaccharides Composed of Sodium Alginate and Carrageenan: The Effect of Annealing on the Separation of Methanol/Water Mixtures

Sang-Gyun Kim, Ki-Sub Lee, Kew-Ho Lee

Membrane and Separation Research Center, Korea Research Institute of Chemical Technology, P.O. Box 107, Yuseong-Gu, Daejeon 305-606, South Korea

Received 17 March 2005; accepted 30 November 2005
DOI 10.1002/app.23903
Published online in Wiley InterScience (www.interscience.wiley.com).

ABSTRACT: Through the complexation of two anionic polysaccharide blends composed of sodium alginate and carrageenan with divalent calcium ions, polyelectrolyte complex membranes were prepared. The effects of annealing on the structure of the polyelectrolyte complex membranes and on their performance at removing water from a methanol mixture were investigated and discussed. The annealed membranes exhibited a change in their crystallinity. The change was due to a rearrangement of polymer chains, which was induced by a deformation of the chelate structure and intramolecular or intermolecular interactions between the polysaccharides. Because of the effects of annealing on the resulting membranes, water components almost penetrated the membranes to the permeate side in the vapor permeation process. Moreover, the membrane performances were gradually enhanced as the operating temperature increased. © 2006 Wiley Periodicals, Inc. J Appl Polym Sci 102: 5781–5788, 2006

Key words: membranes; metal-polymer complexes; polyelectrolytes; polysaccharides

INTRODUCTION

Pervaporation or vapor permeation is a very useful membrane separation technique for separating organic liquid mixtures, such as azeotropic mixtures and mixtures with close boiling points. Because the technique saves more energy than a conventional distillation process, it is especially useful for dehydrating aqueous alcohol mixtures.[1–4] However, given that organic mixtures come directly into contact with the polymer membrane in pervaporation processes, the performance of the membranes is often influenced by the physical and chemical properties of the membranes and the coupling phenomena between permeants. Accordingly, vapor permeation has been introduced as a membrane separation technique to overcome the disadvantages of the pervaporation process.

Vapor permeation has an advantage. That is, because no phase change occurs during permeation from the feed to the permeate side, the problems of supplying the heat of vaporization in the separation process are avoided. As a result, in contrast to the pervaporation process, most hydrophilic membranes in the vapor permeation process yield a higher separation factor and a lower permeation rate when hydrating organic mixtures. For this reason, a plasticizing phenomenon is induced by the permeants on the membrane, and a coupling effect occurs between the permeant molecules. Nevertheless, most hydrophilic membranes have difficulty separating aqueous methanol mixtures because the physicochemical properties between them are the same. Accordingly, in up-to-date research, there is a tendency to remove the methanol component from aqueous solutions with hydrophobic or organophilic membranes, such as silicalite- or zeolite-filled polymers and polybutadiene.[5–9]

On the other hand, it has been reported in recent studies that hydrophilic zeolite membranes can successfully remove water from a mixture of methanol or ethanol through pervaporation and vapor permeation because of their molecular-sized pores and their adsorption properties. In addition, Mitsui Engineering and Shipbuilding Co., Ltd., in cooperation with Yamaguchi University, has developed a zeolite NaA membrane module for solvent dewatering;[10] however, no effective polymeric membranes have yet been developed for dehydrating aqueous methanol solutions.

Hence, the objective of this study was to prepare polymeric membranes that could effectively separate methanol and water mixtures in a vapor permeation process. It was previously announced by us that we had developed polyelectrolyte complex (PEC) membranes with ionic polysaccharides such as sodium alginate (SA) and chitosan and that these membranes

Correspondence to: K.-H. Lee (khlee@krict.re.kr).

exhibited an excellent pervaporation performance for the dehydration of most aqueous alcohol solutions except methanol/water mixtures.[11] On the basis of previous work and with the aid of molecular modeling techniques, we deduced that the desorption rate, which is related to the retention time of the permeants in the membrane, is a predominant factor in organic matter of similar physicochemical properties and molecular size. We found that the retention time of the methanol molecule at the diffusion step should be shorter than the retention time of the water molecule because of the strong interaction between the water molecules and the polar groups of the membrane. However, because of the physicochemical properties of the methanol molecule, such as its hydrophilic surface and hydrogen-bonding ability, its retention time is in fact shorter than that of the water molecule.

Accordingly, we attempted to use morphological control methods at the molecular level to develop a membrane that could effectively remove water from methanol mixtures. In using these methods, we considered the structural characteristics and permeation behavior of zeolite membranes. First, PEC membranes with two anionic polysaccharides composed of SA and carrageenan (CG) were prepared, and then they were crosslinked by divalent calcium ions. Finally, their morphology was modified with an annealing method as a posttreatment.

EXPERIMENTAL

Materials

SA and CG were purchased from Aldrich, Inc. (Milwaukee, WI, USA), and the methanol (a guaranteed reagent) was supplied by Merck (Darmstadt, Germany). Calcium chloride dihydrate (extra-pure-grade) was purchased from Junsei Chemical Co. (Tokyo, Japan). We used ultrapure deionized water, and we used all the chemicals without further purification.

Membrane preparation

SA and CG were dissolved in deionized water to form a homogeneous solution of 2 wt % polymer. The mixtures of the SA–CG solution, which had weight ratios of 95 : 05, 90 : 10, and 80 : 20, were stirred at room temperature for 12 h. The mixed solutions were cast onto a glass plate to give a thickness of 80 μm and then dried at room temperature for 24 h in a dust-free, environmentally controlled chamber. The dried films were immersed in a 5 wt % $CaCl_2$ aqueous solution for 12 h, washed several times with pure water to eliminate any possible residual calcium ions, and dried at room temperature. Finally, we prepared the annealed complex membranes by heating the complex membranes in a convection oven at 110°C for 4 h.

Membrane characterization

The chemical structures of the prepared membranes were characterized with a Fourier transform infrared (FTIR) spectroscope (Digilab FTS-80, Bio-Rad, Richmond, CA). The change in the membrane morphology was investigated with a wide-angle X-ray diffractometer (model D/MAX IIIB; Rigaku, Tokyo, Japan) and a scintillation counter detector that used Cu Kα radiation as a source. The angles (2θ) ranged from 2 to 50°. The thermal properties of the prepared membranes were measured with a model 2950 thermogravimetric analyzer (TA Instruments, Wilmington, DE, USA). The differential scanning calorimetry (DSC) measurements were taken with a DuPont 9000 thermal analyzer with liquid nitrogen for cooling and a heating rate of 10°C/min in a temperature range of 30–300°C. The thermogravimetric analysis (TGA) thermograms were obtained with a DuPont 951 thermogravimetric analyzer with a heating rate of 10°C/min in a temperature range of 30–800°C under a continuous nitrogen flow of 50 mL/min.

Vapor permeation test

Figure 1 shows the schematic vapor permeation apparatus. Basically, the apparatus had the same frame as the pervaporation equipment described elsewhere, except

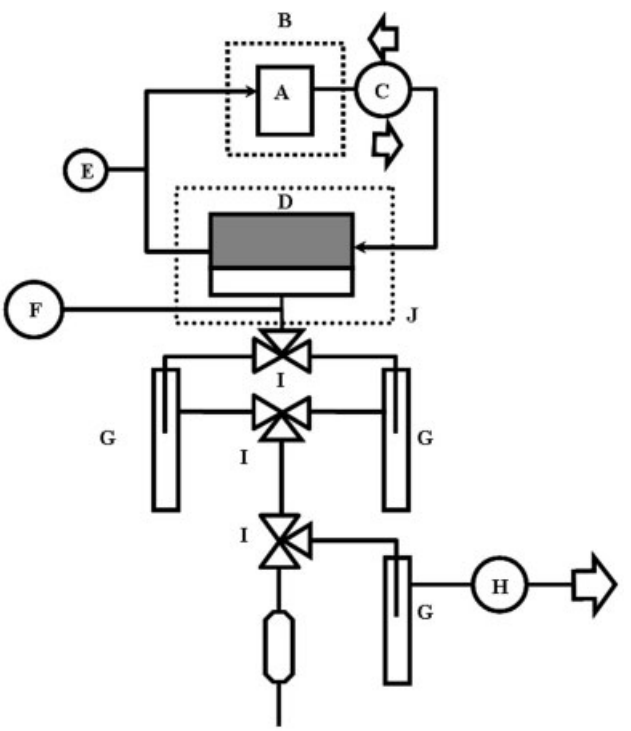

Figure 1 Schematic representation of the vapor permeation device: (A) feed tank, (B) heating controller, (C) pump, (D) vapor permeation cell, (E) temperature indicator, (F) pressure indicator, (G) cold trap, (H) vacuum pump, (I) three-way vacuum valve, and (J) convection oven.

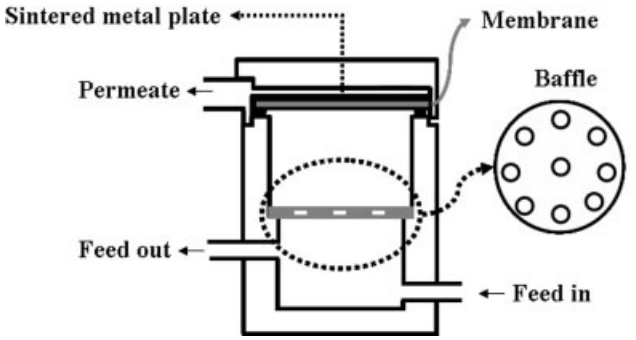

Figure 2 Vapor permeation cell.

for the membrane cell. As shown in Figure 2, the membrane cell was designed to produce a saturated vapor of a feed liquid at a feed temperature. The effective membrane area was 19.6 cm^2. The feed mixture was circulated from the feed tank, which had a capacity of 2.5 L, to the membrane cell. The feed mixture entered the cell through the lower opening and exited the cell through the higher opening; in addition, the flow rate was sufficient to prevent the level of the liquid from rising above the position of the higher opening.

While the feed mixture was circulated through the membrane cell, a saturated vapor was produced in the cell in equilibrium with the feed mixture at the feed temperature. The cell was placed in a heating oven. To prevent the vapor from condensing in the cell, the heating oven was used to control the temperature of the vapor at 5°C or higher above the feed temperature. The feed tank was wrapped with heating tape to heat the feed mixture, and the temperature was controlled by a proportional-integral-derivative (PID) temperature controller with an accuracy of 0.5°C. The permeation vapor was captured in a cold trap by liquid nitrogen in a given time interval. It was then heated to room temperature and weighed to determine the flux. The separation analysis was conducted with a gas chromatographer (model GC 14B, Shimadzu, Kyto, Japan), which was equipped with a column packed with Porapak-Q and with a thermal conductivity detector. The separation factor ($\alpha_{water}/_{alcohol}$) was calculated with the following equation:

$$\alpha_{water/alcohol} = (Y_{water}/Y_{alcohol})/(X_{water}/X_{alcohol})$$

where X and Y are the weight fractions of each component in the feed and permeate, respectively.

RESULTS AND DISCUSSION

Figure 3 shows the results of the FTIR analysis of the blended and complex membranes made with SA and CG. As shown in Figure 3(a), the blended membrane is characterized by the following: a S=O stretch peak in the sulfate group of CG at 1232 cm^{-1}, COO^- antisymmetric stretch peaks and in-plane OH bending peaks in carboxyl groups of SA at 1603 and 1411 cm^{-1}, and OH stretch peaks or hydrogen-bonded OH stretch peaks between the polysaccharides at 3100–3600 cm^{-1}. In contrast, the hydrogen-bonded peak of the complex membranes at 3200–3000 cm^{-1} decreases and shifts to an upper wave number. This difference can be explained in terms of specific intermolecular cooperative interactions between the calcium ion and the guluronate segments (G-blocks) of the alginate; that is, as shown in Figure 4, the calcium ions can occupy the interstices in these structures.[12]

We thought the chelation of the calcium ions would interfere in the intermolecular hydrogen bonding of SA and CG. However, because of a decrease in the

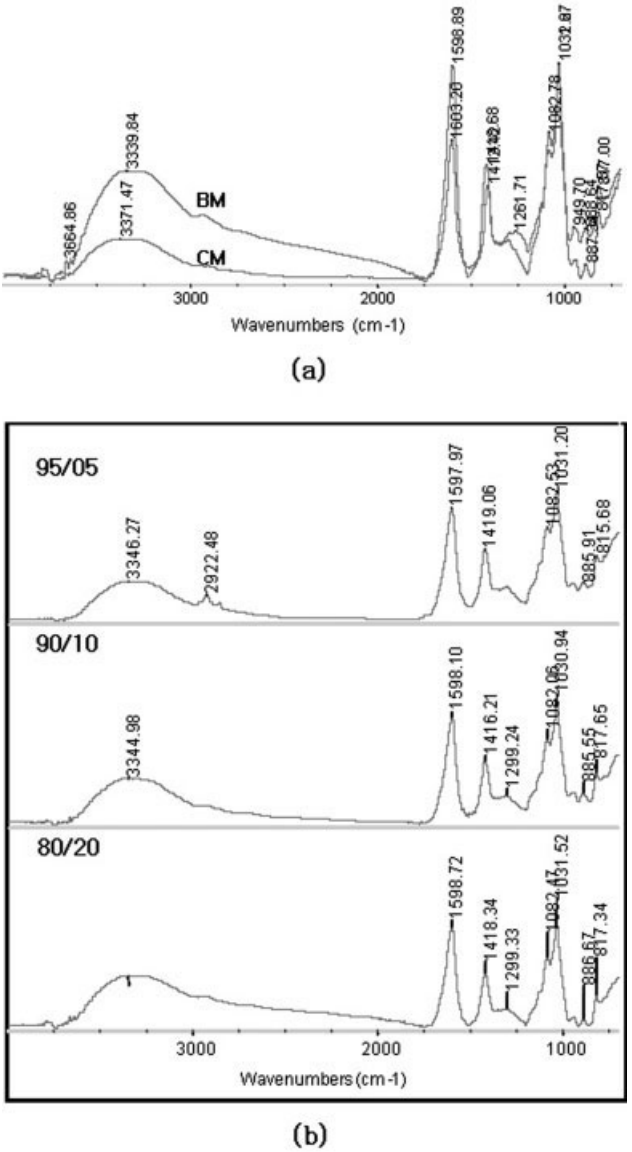

Figure 3 FTIR results of the membranes: (a) spectra for the blended membrane (BM) and complexed membrane (CM) and (b) spectra for the complexed membrane as a function of the SA/CG ratio.

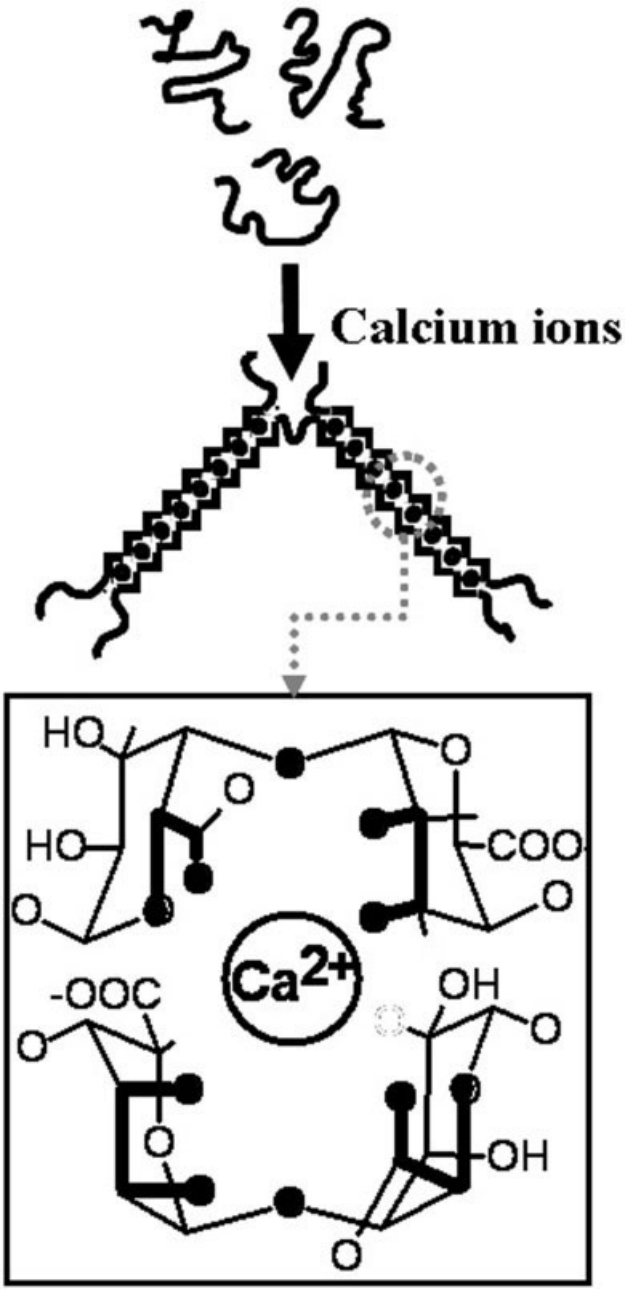

Figure 4 Schematic representation of chelate formation by calcium ion.

chelate formation with calcium ions, as well as the steric hindrance of the CG sulfate groups in the membrane, which can be seen in Figure 3(b), the hydrogen-bonded stretch mode increases as the CG content in the complex membranes increases. From this result, it is deduced that the morphology of the resulting membranes has a more compact network structure. Furthermore, as the CG content increases, there is less chain mobility because of the enhanced intermolecular hydrogen bonding of the polysaccharides.

The X-ray diffraction (XRD) patterns of the prepared membranes were also studied to observe the morphological changes during the chelate formation with calcium ions and the intermolecular hydrogen-bonding interaction. Generally, SA is an anionic polysaccharide with an amorphous morphology, whereas CG has a crystalline morphology because of the domain structure, in which a limited number of chains form an intermolecular double helix.[13–15] Thus, as shown in Figure 5(a), the crystal structure of CG occurs in the blended membrane when 2θ is near 8°.

In contrast, the XRD patterns show a decrease in the amorphousness of the membranes chelated with calcium ions at the same 2θ value of CG. There is

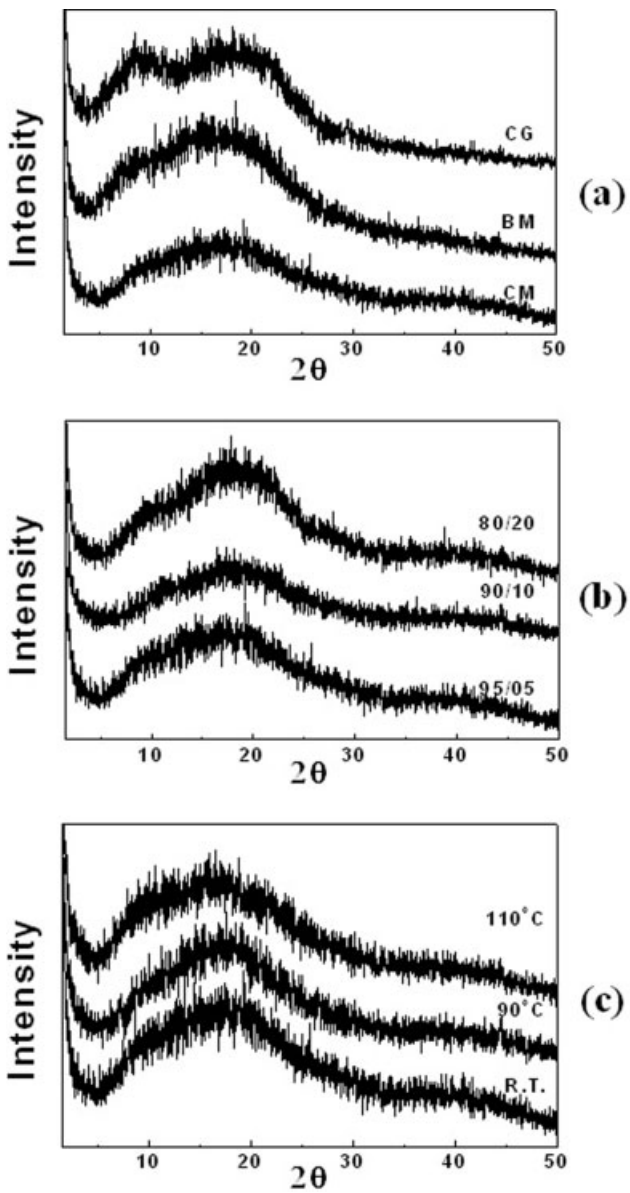

Figure 5 XRD results of the membranes: (a) XRD patterns for the pure CG membrane, blended membrane (BM), and complexed membrane (CM); (b) XRD patterns for CM as a function of the CG content; and (c) XRD results for the annealed membranes as a function of the annealing temperature.

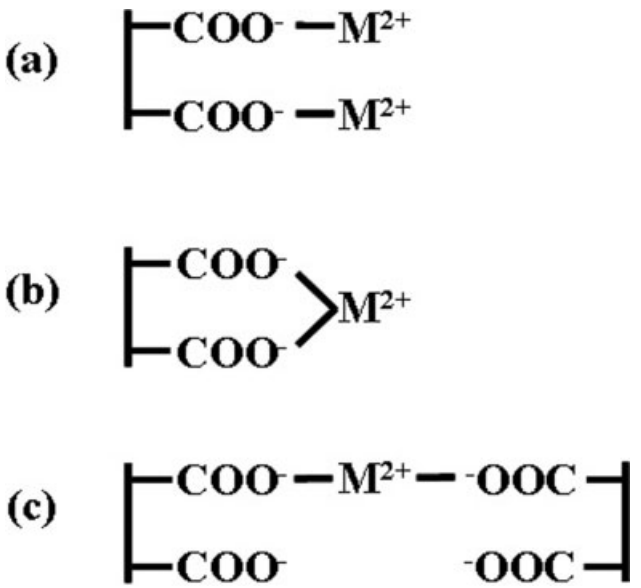

Figure 6 Schematic representation of the chelate structures by divalent metal ions: (a) pendent half-salt, (b) in-chain disalt, and (c) cross-chain disalt.

also an upward shift in the amorphous regions of 16°, and there is a change in the *d*-spacings from 5.4 to 4.9 Å. As the CG content in the complex membranes increases, the *d*-spacings of the amorphous region gradually decrease to 4.8 Å, and as shown in Figure 5(b), there is a shift to a higher 2θ value than 5 wt %. This phenomenon is due to the chelate formation with calcium ions in the G-blocks of SA and the ionic crosslinking between the CG sulfate groups or between anionic groups such as CG sulfate and SA carboxylate.

Some researchers have mentioned that in principle, divalent cations, such as Ca^{2+} and Zn^{2+}, exist as six-coordinate species.[16,17] Furthermore, as shown in Figure 4, the oxygen atoms of SA can coordinate to the calcium during the chelate formation. As a result, the oxygen atoms that participate in the chelation reaction make it difficult for the hydrogen bonding to interact intermolecularly between the polysaccharides. In addition, as shown in Figure 6, the coordination of the divalent cations can exist as three types of fused structures: pendent half-salts, as in-chain disalts, and as cross-chain disalts.[15] Because of this coordination, the helical domains of CG form a crystalline peak when 2θ is near 8°, although this phenomenon might be hindered by the intermolecular interaction of SA and CG as an ionic crosslinking. Consequently, the decrease in the crystalline regions of the blended membrane is due to the ionic crosslinking of SA and CG and to the reduction in the extent of hydrogen bonding.

Figure 7 shows the exothermic peaks in the complex membrane at 186°C. These peaks could be evidence of the aforementioned specific interactions because, depending on the CG content, the peaks shift gradually to a lower temperature, and the heat of fusion increases from 4.1 to 19.97 J/g. In other words, as shown in Figure 6, because the depression of the exothermic temperature is attributed to the miscibility or intermolecular interaction of SA and CG, it is deduced that the ionic crosslinking is composed of the cross-chain type of disalt.

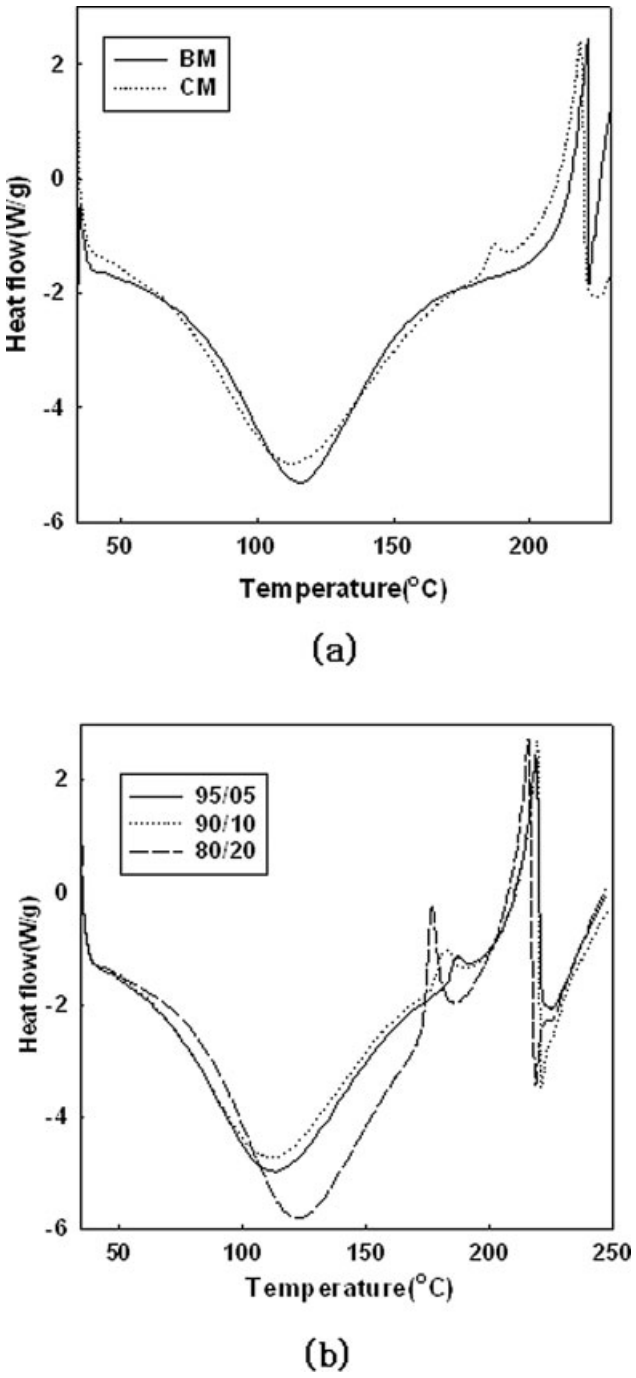

Figure 7 DSC results for the membranes: (a) DSC curves for the blended membrane (BM) and complexed membrane (CM) and (b) DSC curves for CM as a function of the CG content.

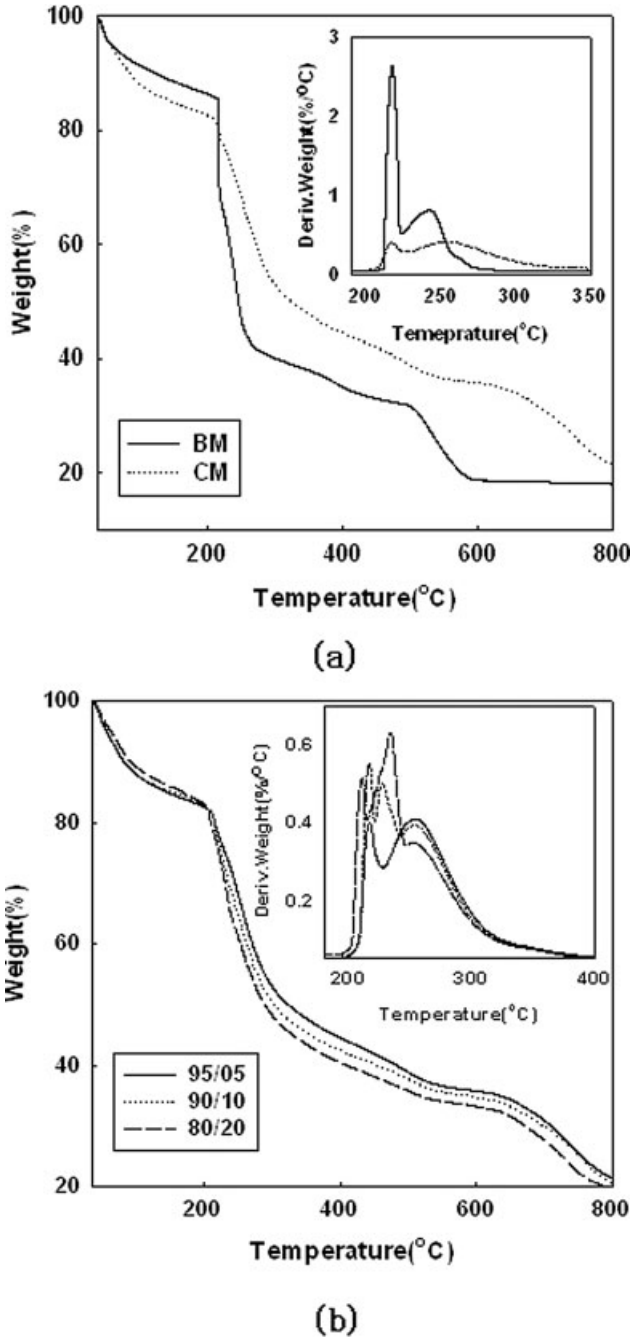

Figure 8 TGA and DTG results for the membranes: (a) TGA and DTG curves for the blended membrane (BM) and complexed membrane (CM) and (b) TGA and DTG curves for CM as a function of the CG content.

This observation corresponds to the thermal degradation behavior revealed in the results of TGA, which are shown in Figure 8. As shown in the differential thermogravimetry (DTG) curves of Figure 8(a), the membranes have two decomposition temperature traces at 220 and 300°C. Furthermore, in comparison with the decomposition behavior of the blended membrane, the complex membrane appears in the weight-loss patterns of a slow-moving rate at a higher temperature. Therefore, it is concluded that this phenomenon is due to an increase in the thermal stability, which is caused by ionic crosslinking with the chelate formation in the G-blocks of SA.

On the basis of the decomposition pattern results of Figure 8(b), when the CG content increases, the membranes exhibit a new degradation peak at 225°C, whereas the peak at 210°C shifts to a lower temperature. Moreover, the patterns at 250°C gradually decrease. Therefore, it is assumed that the weight loss at 225°C is related to the degradation of the chelate structures, as shown in Figure 6(c).

However, when the complex membranes are modified thermally by an annealing method at 90 and 110°C, the thermal decomposition patterns of the resulting membranes exhibit an increase in the

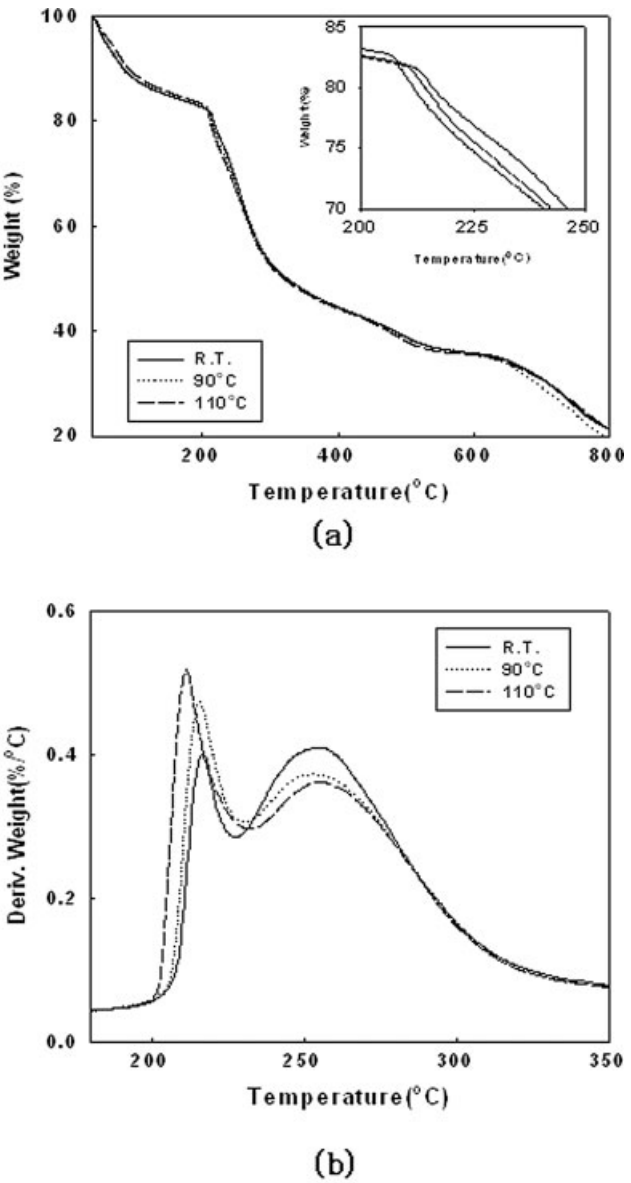

Figure 9 (a) TGA and (b) DTG results for the annealed membranes as a function of the annealing temperature.

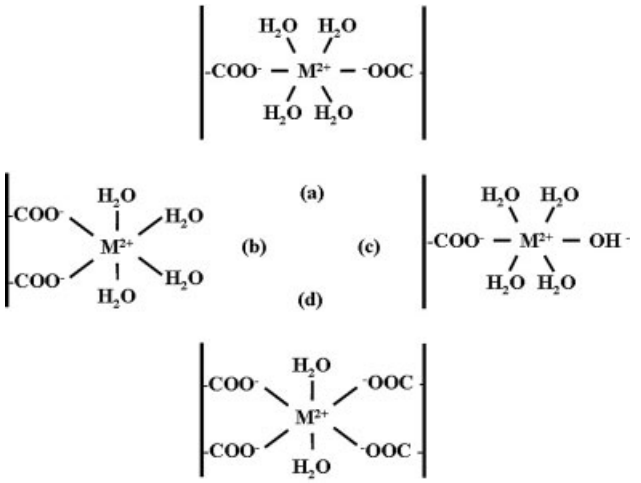

Figure 10 Schematics representation for the possible chelate structures related to six-coordinate divalent metal ions.

exothermic peak patterns at approximately 210°C and a reduction of the peaks at 300°C, as shown in Figure 9. Furthermore, as the annealing temperature increases, the weight loss in the first stage (between 170 and 231°C) increases from 7 to 12%, and there are decreasing patterns in the weight loss of the second stage between 217 and 415°C (from 32.7 to 28.5%).

This behavior might be due to the deformation of the chelate form by means of the dehydration of water molecules around the calcium ions, as shown in Figure 10.[15] It might also be due to the transformation of the CG morphology by the thermally induced changes in the order–disorder transition. This observation is supported by the XRD results of the membranes in Figure 5(c) because the intensity of the peak at $2\theta = 8^\circ$ increases and the amorphous region of 17° shifts gradually to 16°. Consequently, the weight loss for the decomposition in the first and second stages is obviously related to the morphological transformation of the resulting membrane. In addition, the morphological transformation is induced by a deformation of the chelate segments and by the rearrangement of the polymer chains during the annealing process. Moreover, the alternation in the structural viewpoint may result in a denser structure and a lower free volume in the internal membrane than in the unmodified membranes.

Figure 11(a) shows the effect of the annealing on the permeation rate and the methanol concentrations in the permeate of the nonannealed complex membranes. The effect is shown as a function of the CG content for the separation of 80 : 20 (w/w) methanol/water mixtures when vapor permeation is used. For nonannealed complex membranes, the permselectivity for separating methanol/water mixtures is generally very low, although the permeation rates are high as a whole. As the CG content in the blend ratio increases, the permeation rates of the membranes decrease gradually but improve its permselectivity. In this case, however, the permselectivity corresponds to the permeation behavior toward morphological changes that are related to the increase in

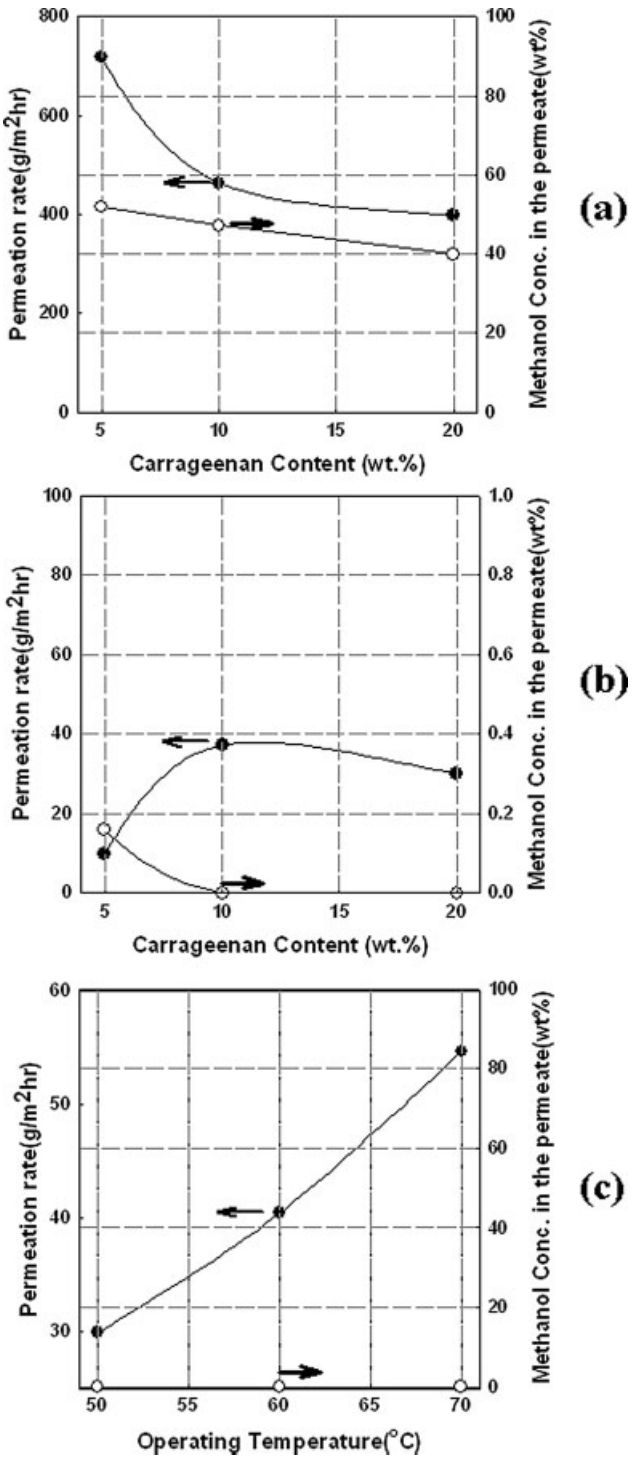

Figure 11 Permeation results for (a) the nonannealed membrane, (b) the annealed membrane, and (c) the annealed membrane as a function of the operating temperature for the separation of 80/20 (w/w) methanol/water mixtures.

intramolecular or intermolecular hydrogen-bonded structures. This phenomenon, which is apparent in the results of the FTIR spectra and the XRD patterns, is attributable to the higher values of permselectivity. Moreover, the lowest permeation rate can be obtained in correspondence with the lower chain mobility and the denser structure.

Figure 11(b), on the other hand, shows that the annealed complex membranes greatly reduce the permeation rates and the methanol concentrations in the permeate at the same time and that the water components almost penetrate the resulting membrane to the permeate side. Although the permeation rates are very low, the permeation results contrast with the trend of nonannealed complex membranes.

The results may have also been affected by an increase in the free volume between the polymer chains because of the steric hindrance of the CG sulfate groups on the membranes. In addition, as shown in Figure 11(c), as the operating temperature increases, the permeation rate of the annealed complex membranes gradually improves without the permselectivity decreasing. According to the free-volume theory, when the operating temperature increases, the thermal motion of the polymer chain generally increases and generates more free volume in the polymer matrix to facilitate the sorption and diffusion of permeants in the membrane.

As a result, the overall permeation behavior tends to increase the permeation rate and to reduce the permselectivity. However, although the permeation behavior of the annealed complex membrane greatly increases the permeation of the water component, the permeation of methanol remains unchanged. The annealed membranes that are complexed with calcium ions act as molecular sieves in the separation of methanol and water mixtures because of the shrinkage of the free volume between the polymer chains and the chelate segments.

CONCLUSIONS

To separate methanol/water mixtures, an annealing method was used to modify the morphology of polyelectrolyte membranes that were composed of SA and CG and complexed with divalent calcium ions. As a result, water components almost penetrated the membrane to the permeate side, and the membrane performance was gradually enhanced as the operating temperature increased. This phenomenon was due to the change in the morphology, which was induced by the rearrangement of the polymer chains that were involved in the deformation of the chelate structure and intramolecular or intermolecular interactions such as hydrogen bonding. From these results, it was also deduced that the annealing of complex membranes acts as a molecular sieve, which can be modulated by the shrinkage of the free volume between the polymer chains from a structural viewpoint.

References

1. Huang, R. Y. M. Pervaporation Membrane Separation Processes; Elsevier: Amsterdam, 1991.
2. Sander, U.; Janssen, H. J Membr Sci 1991, 61, 113.
3. Will, B.; Lichtentthaler, R. N. J Membr Sci 1992, 68, 119.
4. Schehlmann, M. S.; Wiedemann, E.; Lichtentthaler, R. N. J Membr Sci 1995, 107, 277.
5. Yoshikawa, M. M.; Wian, T.; Kuno, S.; Kitao, T. Proceedings of the 6th International Conference on Pervaporation Processes in the Chemical Industry; Bakish Materials: Ottawa, Canada, 1992; p 178.
6. Devaine, K. M.; Meier, A. J.; Slater, C. S. Proceedings of the 7th International Conference on Pervaporation Processes in the Chemical Industry; Bakish Materials: Reno, USA, 1995; p 218.
7. Hennepe, H. J. D.; Mulder, M. H. V.; Smolder, C. A.; Bargerman, D.; Schroder, G. A. T. U.S. Pat. 4,925.563 (1990).
8. Kita, H.; Hori, K.; Okamoto, K. Proceedings of the 7th International Conference on Pervaporation Processes in the Chemical Industry; Bakish Materials: Reno, USA, 1995; p 364.
9. Sano, T.; Yanagishita, H.; Kiyozumi, Y.; Mizukami, F.; Haraya, K. Stud Surf Sci Catal 1994, 84, 1175.
10. Okamoto, K. I.; Kita, H.; Horil, K.; Tananka, K.; Konto, M. Ind Eng Chem Res 2001, 40, 163.
11. Kim, S. G.; Lee, K. S.; Lee, K. H. J Appl Polym Sci, 2005, to appear.
12. Morris, E. R.; Rees, D. A.; Thom, D.; Boyd, J. J Carbohydr Res 1978, 66, 145.
13. Morris, E. R. Br Polym J 1986, 18, 14.
14. Millane, R. P.; Chandrasekaran, R.; Arnott, S.; Dea, I. C. M. Carbohydr Res 1988, 82, 1.
15. Janaswamy, S.; Chandrasekaran, R. Carbohydr Res 2002, 337, 523.
16. Wilson, A. D.; Crisp, S. In Ionic Polymers; Holliday, L., Ed.; Applied Science: London, 1975; Chapter 4.
17. Wilson, A. D.; Crisp, S. Br Polym J 1975, 7, 279.